

Effects of cold plasma treatment on interlayer bonding strength in FFF process

Chin-Cheng Shih^a, Matthew Burnette^a, David Staack^a, Jyhwen Wang^b, Bruce L. Tai^{a,*}

^a Department of Mechanical Engineering, Texas A&M University, College Station, TX, USA

^b Engineering Technology and Industrial Distribution, Texas A&M University, College Station, TX, USA



ARTICLE INFO

Keywords:

Plasma treatment
3D printing
Fused filament fabrication
Bonding strength

ABSTRACT

Fused Filament Fabrication (FFF) is the most popular additive manufacturing method because of its numerous capabilities and relatively low cost. This comes with a trade off as FFF printed parts are typically weak in the layer deposition direction due to insufficient interlayer bonding. This research adopts the method of cold plasma treatment and investigates the potential enhancement of interlayer bonding by altering the printed surface prior to the deposition of the next layer. Polylactic acid (PLA) is used as the printing material, due to its ubiquity in industry. The bonding strength is measured by the shear bond strength test. The results show that bond strength improved over 100% with 30 s of treatment and over 50% with 300 s of treatment. A mechanically polished surface is also included in the comparison for the high surface wettability, but the result shows no improvement. This indicates that wettability may not be the dominant mechanism for enhanced bonding after treatment.

1. Introduction

Fused Filament Fabrication (FFF) is an extrusion-based additive manufacturing (AM) technology, invented in the 1990s [1], which uses a printing head with a continuous filament to fabricate parts additively in a layer-by-layer manner. The printing head can move in two or three dimensions depending on the configuration of the machine. This movement is controlled numerically and determined according to input Stereolithography (.stl) models. Once a layer is finished, the build platform will move for printing the next layer. This process repeats for every layer until the entire model is built. Due to its simplicity and many suitable materials, FFF has been widely used for a variety of applications in both academic and industrial fields. However, the fact that FFF relies on thermally-induced diffusion bonding presents major problems for material anisotropy, which has inhibited the use of FFF in functional parts. FFF-printed parts are typically weaker in the layer deposition direction (*z*-direction) than other orientations. Unlike *x*- and *y*-directions where the bulk material fibers can provide strength, the strength in the *z*-direction solely relies on bonding strength between layers. Ahn et al. (2002) [2] tested the tensile strength on FFF-printed ABS P400 specimens in different orientations. The results showed that tensile strength in the transverse direction is approximately 20 percent

of the strength in the axial direction and 35 percent of the strength in the cross direction. It is known that insufficient interlayer bonding is a result of incomplete diffusion bonding [3,4]. Although enhanced thermal diffusion can be achieved by heating, there exist three major technical challenges. Firstly, FFF only heats up material locally in the nozzle, and the melt begins to cool down and solidify after being extruded and before being laid down on top of a deposited layer. This process causes incomplete diffusion due to insufficient thermal energy being retained in the material [3]. Secondly, since each deposited layer is made of multiple cylindrical extrusion arrays, geometrically produced vacancies between layers can reduce the contact area for diffusion bonding [4]. Lastly, the surface condition may not be active for bonding due to low surface energy, contamination, chemical composition, or weak boundary layers [5].

To mitigate these issues, some researchers proposed optimizing printing parameters to achieve a higher strength [4,6,7], while others looked into external approaches such as material modification, additional steps or external energy application [8–16]. These approaches can be categorized into pre-process, in-process, and post-process. Various groups have tried pre-processing the filament prior to printing. Abourayana et al. (2017) [8] used a barrel atmospheric plasma to treat polymer pellets used for FFF filaments and showed a 22% increase of

* Corresponding author.

E-mail address: btai@tamu.edu (B.L. Tai).

the tensile strength of the printed part. Nguyen et al. (2018) [9] mixed ABS material with acrylonitrile-butadiene rubber, lignin, and carbon fibers to improve both printability and bonding. For in-process treatments, Ravi et al. (2016) [10] used a laser system to locally heat the surface immediately before depositing the next layer to increase thermal diffusion. Similarly, Kishore et al. (2016) [11] preheated the printed layer before the next layer using infrared lamps. Sweeney et al. (2017) [12] invented a special type of filament coated with a thin layer of carbon nanotubes (CNTs) and used microwave heating during printing to improve the overall part strength. For post-process treatments, Shaffer et al. (2014) [13] utilized ionizing radiation to heat treat the printed part to improve bonding strength via enhanced crosslinking. Garg et al. (2017) [14] used acetone vapor to treat FFF-printed parts but produced a marginal reduction in strength. Jo et al. (2018) [15] increased the strength of 3D-printed PLA objects by heat treatment in a heated mold. Li et al. (2018) [16] applied pressure and ultrasonic vibration on 3D-printed parts to increase the part's tensile and bending strengths.

Most of the aforementioned methods use heating to achieve better bonding strength. However, heating can inherently generate defects in printed parts. Localized or high-power heating, for example, can induce part distortion or warpage due to thermal stress, which is known to degrade part dimensional accuracy [17]. Furthermore, pre- and post-processes require additional time and labor, which may reduce the simplicity and convenience of FFF 3D printing. For these reasons, this study presents an in-process and non-heating-based solution, named cold plasma treatment (CPT), to enhance the bonding strength while minimizing heat-induced distortion and defects. CPT is a surface modification technique that utilizes a high voltage and low current non-equilibrium plasma discharge to chemically and physically alter surface properties (to the depth of 50–500 Å) [18,19]. CPT is operated at atmospheric pressure in a non-equilibrium fashion characterized by high-temperature electrons (up to 10,000 °C) and room temperature gas (20 °C–40 °C) [20]. Cold plasma applicators have various geometries configured to provide high voltages and low average currents [21]. Examples include: 1) corona discharge geometries with sharp tips powered by a high voltage DC power, and with an incomplete breakdown of the discharge gap [22,23]; 2) dielectric barrier discharges (DBD), in which one or both high voltage electrodes are covered by an electrically insulating barrier to limit currents [24–26], 3) nanosecond pulsed plasma (NPP) and microsecond pulsed plasma (μ PP) discharges where the external circuit is used to limit discharge power; and 4) plasma jets, in which convection of a gas (typically a noble gas) along with its electrical and transport properties help maintain the non-equilibrium [27]. These various sources have similar global plasma properties, although they vary significantly in their cost, efficiency and ability to maintain non-equilibrium over a wide variety of operating conditions. Aspects of these configurations can also be combined for greater efficacy. Historically DBDs and coronas have been used since the early 1900's in industrial applications for surface modifications. Jets and NPP have gained popularity in research in the last 20 years. In the extrusion-based AM field, Hiroyuki et al. (2016) [20] applied a plasma jet with helium gas for enhanced interlayer bonding. This research adopts a different plasma source which combines aspects of a NPP, a jet, a corona geometry, and a DBD to create a highly non-equilibrium glow discharge.

CPT has been widely used in industry to increase the surface energy of various polymers for enhanced adhesion or bonding [28]. The two major mechanisms of CPT that enhance surface adhesion involve polar group introduction and polymer chain scission. As CPT triggers

oxidation on the polymer surfaces, polar groups with high surface energy such as carbonyl groups will form on surfaces, resulting in a better wettability. This improved wettability prompts liquid to spread along the surface, providing a larger contact area for diffusion bonding. Since polymers are synthesized from numerous long molecular chains joining end to end with only a few dangling ends at the surfaces for further bonding, their adhesion and wettability are poor. CPT can relieve this issue by breaking the polymer chains producing loose ends for bonding by bombarding the polymer surfaces with electrons during the plasma discharge and other radicals. Furthermore, polymeric scission products prompt better interfacial flow and inter-diffusion due to their lower molecular weight, lower glass transition temperature, and lower viscosity, so treated surfaces require less thermal energy (lower temperature) for bonding [5,29,30].

The objective of this paper is to determine the improvement of interlayer bonding of FFF via CPT and to investigate the dominant mechanism of enhanced bonding. To achieve this, different treatment times along with mechanically polished and unpolished samples are compared in this work. Mechanical polishing is included as it also changes the surface wettability due to the interactions between liquid surface tension and surface texture. This is, therefore, used to study the significance of wettability in interlayer bonding strength alone as well as to analyze the combined effect with CPT. To organize the whole study in this paper, Section 2 summarizes the materials and methods for specimen preparation, cold plasma treatment, and bonding strength testing. Section 3 details the experimental results. Section 4 provides discussion of the results. Section 5 draws the conclusions from this study.

2. Material and methods

2.1. Experimental setup and specimen preparation

Polylactic acid (PLA) was selected as the testing material as it is a common thermoplastic in FFF with widespread accessibility and less dimensional distortion after printing. A FFF 3D printer, Dreamer (Flashforge, Zhejiang, China) and standard 1.75 mm PLA filaments in blue were used to fabricate specimens. Slicing software, Simplify3D (Simplify3D, Cincinnati, OH), was used to arrange the printing parameters and tool paths. The design of specimen geometry included two sections, substrate, and top layer, as shown in Fig. 1. The substrate was

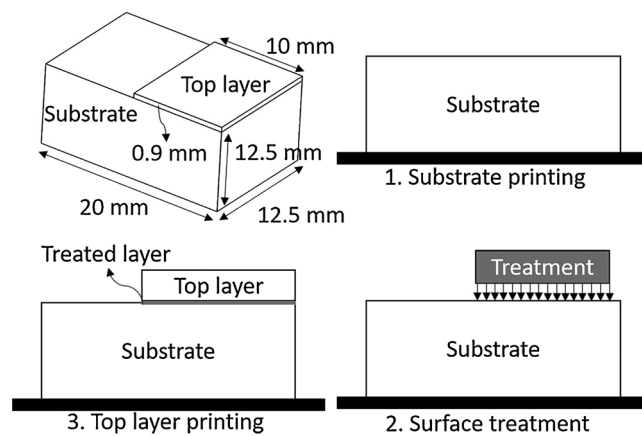


Fig. 1. Dimensions and the three steps of specimen preparation for the shear bond test.

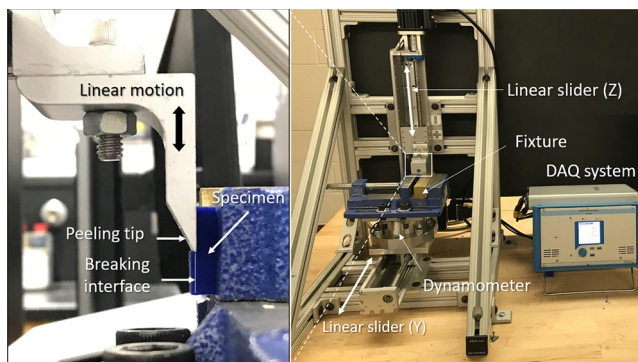


Fig. 2. The setup for shear bond test to determine the interlayer bonding strength.

20 mm by 12.5 mm by 12.5 mm, and the top layer was a thin layer meant to be sheared off to determine the bonding strength. The specimens were made following three-step procedures. Once the substrate was printed, the printing process was paused, and the entire printing platform was removed to conduct surface treatment away from the machine in order to avoid contamination and electromagnetic interference from the CPT. After the treatment, the platform was installed back in the 3D printer to continue the printing of the top layer. This way ensured a consistent layer thickness across the treated interfacial layer. If the substrate and top layer were printed separately, inconsistent layer thickness could be created due to machine zeroing error. In addition, the re-installed platform must stay in the machine for at least 30 min. to allow the printed part to reach a steady-state temperature around 38.3 °C in order to avoid temperature discrepancy with the baseline printing. Note the heat-induced dimensional error is negligible given a small thermal expansion coefficient (4.1×10^{-7} m/m) of PLA and little shrinkage. Finally, the complete specimen was sent to the testing apparatus.

A self-developed apparatus, shown in Fig. 2, used a sharp tip to shear and peel the top layer off from the substrate. The shearing force was measured using a dynamometer that could capture a rapid force response. The measured force was used to represent the interlayer bonding strength. This method was adopted from the shear bond strength test of dental composites [31] because of the simplicity, small bonding area, and specimen required as compared to standard adhesion or tension tests, in which the material anisotropy may create weak spots in a larger specimen. Other components in the apparatus included a fixture on the dynamometer to secure the specimen and a numerically controlled linear slider for a quasi-static peeling rate at 12.5 mm/min. The data acquisition (DAQ) system was used to transfer high-frequency data at a sample rate of 10 Hz from the dynamometer to the computer in real time.

Using an untreated sample as the baseline, the four surface conditions are listed in Table 1. The results were expected to unveil the

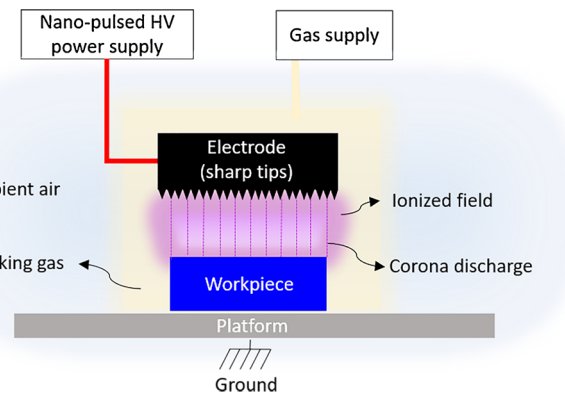


Fig. 3. Schematic of Cold Plasma Treatment (CPT) mechanism.

effects of CPT on interlayer bonding and the dominant bonding mechanism being wettability or the continuous cross-linking via polymer chain scission. The only variable in CPT was the treatment time. It was hypothesized that a longer treatment resulted in a stronger bonding; thus, two substantially different time durations, 30 s and 300 s, were selected. For mechanical polishing, only one grit size was selected since the main purpose was to test the effect of wettability (i.e. high vs. low) by altering the surface profile. Further, Test #4 was to check if combining polishing and CPT can result in a better performance than CPT alone. Each condition contained five specimens to ensure adequate statistical power for comparison. The details of the surface treatment procedures are presented in the next section.

2.2. Surface treatments and conditions

The configuration of the CPT is shown schematically in Fig. 3 and the actual setup is shown in Fig. 4. The CPT system is composed of a power supply, electrode, electrode holder, adjustable platform, and gas supply. A high voltage nanosecond pulser, FPG 30-N (FID GmbH, Burbach, Germany), was used as the power supply with capabilities of outputting a maximum voltage of 30 kV, pulse width of 3 ns, and a maximum pulse frequency of 10 kHz. A stainless-steel electrode composed of sharp tips and gas spacers was connected to the power supply to produce a dielectric barrier discharge. The sharp tips were made of multiple 0.6 mm thin sheets with a serrated profile machined by electrical discharge machining (EDM), as shown in the close-up view in Fig. 4. The tips are spaced every 0.5 mm across a sheet with 0.4 mm

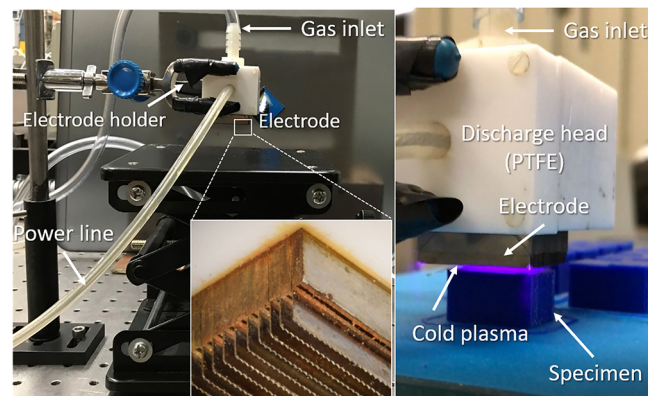


Fig. 4. The setup of CPT system.

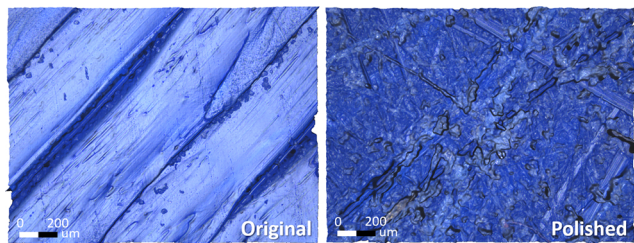
Table 1
Four treatment conditions of specimens.

| Tests | Conditions | Notations |
|-----------------|-------------------------------------|-----------|
| Short CPT | 30 s plasma treatment | CPT30 |
| Long CPT | 300 s plasma treatment | CPT300 |
| Polishing | #180 grits | Polished |
| Polishing + CPT | #180 grits and then 300 s treatment | P + CPT |

Table 2

The working parameters of CPT.

| Plasma Working Parameters | |
|---------------------------|-----------------|
| Voltage (kV) | 20 |
| Frequency (kHz) | 2 |
| Gas (L/min) | 2.5 (Helium) |
| Discharge distance (mm) | ~1 |
| Pressure | Ambient (1 atm) |
| Temperature | Room (22 °C) |

**Fig. 5.** Surface geometries of (a) as-printed and (b) polished PLA.

inter-sheet spacing. The spacers were machined by EDM with a special configuration and inserted between the serrated sheets to allow gas flow. The PTFE (Teflon) block provided housing for the electrode and for transporting the working gas to the electrode. The array of sharp tips is essential to producing large and uniform plasma discharge, and the gas flow kept the temperature low due to the electrical and thermal properties of helium and forced convection.

The following working parameters, shown in **Table 2**, were set to be fixed across all samples in this study. The CPT was working under ambient pressure and at room temperature and humidity (around 22 °C and 60% humidity). The voltage was set at 20 kV, and the frequency was set at 2 kHz. Helium gas was used as the working gas. The measured vibrational temperature was found to be around 3100 K and the rotational temperature was approximately 460 K in this plasma using the 2nd positive system of nitrogen and SpecAir for modeling [32,33]. The discharge distance, the gap between the electrode and the working part, was approximately 1 mm from the tips for the best performance, beyond or below which the plasma did not initiate or became too intense on the surface. In this study, the only independent variable is the discharge time (0, 30 s, and 300 s) to observe the effect on bonding

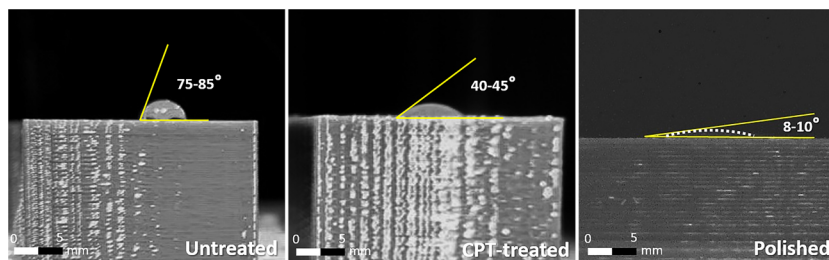
performance.

The mechanical polishing was conducted with sandpaper manually without directionality. Sandpaper with a grit size of 180 was attached on a flat guide plate to grind the target surface gently to ensure an even and uniform surface. The polished surface and residue were cleaned with high-pressure compressive air. The surface roughness was checked using an optical 3D profilometer, InfiniteFocus (Alicona, Graz, Austria), and the default cutoff length of 0.212 mm at multiple spots until consistent roughness value (R_a) was reached and no extrusion marks were observed, as shown in **Fig. 5**. Additionally, the removed surface layer was controlled at 0.1 mm and this height difference was programmed into the 3D printer to compensate for the following layer. Note that the polished surface, in fact, became rougher in terms of R_a (4.98 vs. 1.89 μm) because the surface profile transformed from waviness to the roughness scale.

Before conducting the shear bond test, the specimens were tested for their wettability by the contact angle of water droplet based on ASTM standard (D7334-08) [34]. **Fig. 6** shows the results of the contact angle. The purpose was to ensure that both CPT and mechanical polishing produced high surface wettability. As seen, the untreated baseline surface had a contact angle higher than 75°, that of CPT is around 40–45°, and that of the mechanically polished surface is less than 10°. It is important to note that the wetting effect appears very quickly after CPT and remains nearly constant with respect to treatment time. Both the 30 s and 300 s treatments have a similar contact angle. The mechanically polished surface had the best wetting condition among all, and thus was ideal to be used for comparing the wettability effect in bonding strength.

3. Experimental results

The force data for the CPT30 and CPT300 samples from the shear bond tests are shown in **Fig. 7**, where the peak force of each data represents the bonding strength. For comparison purposes, the untreated specimens are also plotted. As shown, the bonding strengths are significantly improved with CPT. The peak forces of both CPT30 (from 447 to 506 N) and CPT300 (from 272 to 380 N) are repeatedly greater than that of the baseline (from 113 to 237 N). In addition, the baseline specimens experience rapid force drop after the peak force, which indicates a fast crack propagation in brittle materials. In contrast, the force drops for the CPT specimens are progressive, indicating a higher toughness of the interface. Since the shearing rate is constant, the area below each curve represents the energy required to remove the entire top layer. Another interesting finding is that, in the comparison between CPT30 and CPT300 samples, the force values of CPT30 are greater than those of CPT300. This result shows that the bonding

**Fig. 6.** Contact angle measurement of specimens with different surface conditions (a) as-printed, (b) CPT, and (c) polished (the droplet boundary is highlighted with dashed line for the low image contrast.).

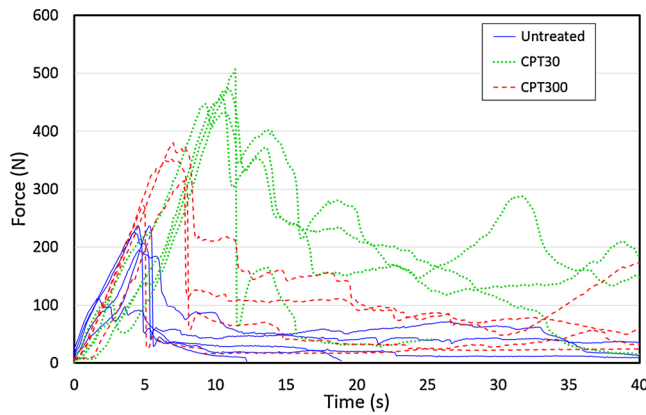


Fig. 7. Force response with respect to time - Untreated, CPT30, and CPT300.

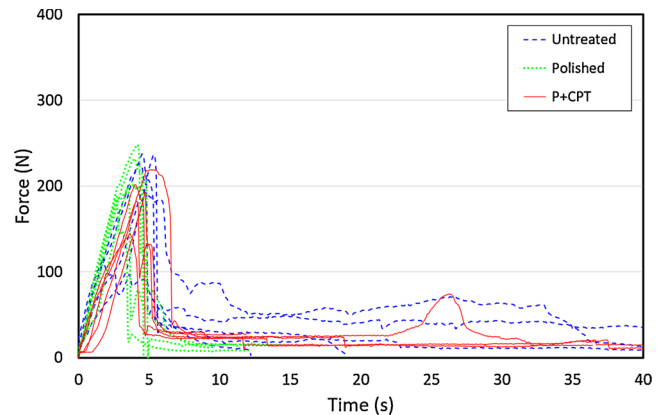


Fig. 9. Force response with respect to time - Untreated, Polished, and P + CPT.

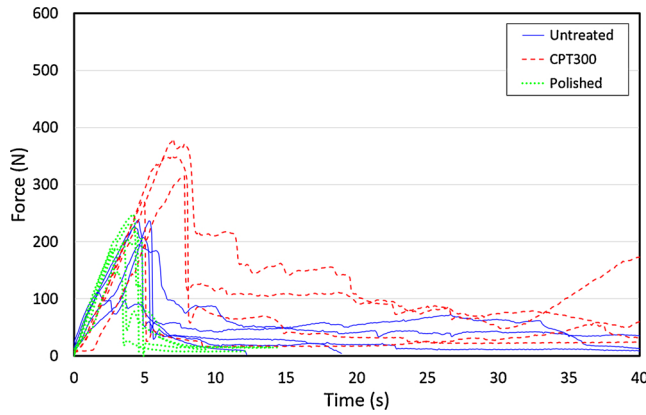


Fig. 8. Force response with respect to time - Untreated, CPT300, and Polished.

strength is not positively proportional to the treating time.

To understand the role of wettability in bonding strength, three test results are studied and compared in Fig. 8, including the baseline, CPT300, and the polished case. For clarification, the results of baseline and CPT specimens are retrieved from the same data set in the previous figure. As can be seen, the CPT300 specimens are the strongest among all. The polished ones, with forces ranging from 188 to 232 N, appear to be similar to the baseline in terms of the peak force and are overall weaker than CPT300. Also, the polished ones have a faster force reduction (after the peak) than those of the baseline despite similar peak forces. This result indicates that mechanical polishing may reduce the bonding toughness.

The third set of results, including baseline, polished, and P + CPT, are compared to investigate the combined effects of two treatments in this study, as shown in Fig. 9. The results show no significant difference among all three tests in terms of the peak force. However, the continuous shearing forces of P + CPT indicate a slightly higher toughness than polished ones, while the baseline remains the toughest. These results show that the negative effect of polishing can overwrite the enhanced adhesion from CPT. CPT cannot further improve the bonding strength after the surface is polished.

The averages of the peak shear-bond forces of all tests are calculated and presented in Fig. 10. The error bars represent the standard error. Based on statistical analysis, CPT300, CPT30, and the baseline are statistically different among each other (p -value < 0.05), whereas polished, P + CPT, and the baseline are considered not statistically different (p -value > 0.05). Considering the baseline bonding strength, CPT30 improves the bonding strength by 134% on average, followed by CPT300 at 63%.

Lastly, the fracture surfaces were observed under an optical microscope to compare the treated effects on the interfaces, as shown in Fig. 11. Stress whitening, also known as crazing, can be seen on both CPT specimens. Stress whitening occurs when thermoplastic polymers are under an excessive tensile load, which causes the formation of microvoids due to the movement of molecular chains, thus changing the material refractive index [35]. Therefore, the degree of stress whitening can reflect the level of bonding force between layers after delamination. CPT 30 shows clear white striations that align with the deposited filament extrusions, indicating a strong bonding between the deposited material and base layer. CPT 300 shows some stress whitening regions, but they are not as many and as well-distributed as those in CPT 30. Such a difference is the evidence of the lower bonding force of CPT 300. The untreated, polished, and P + CPT specimens show no stress

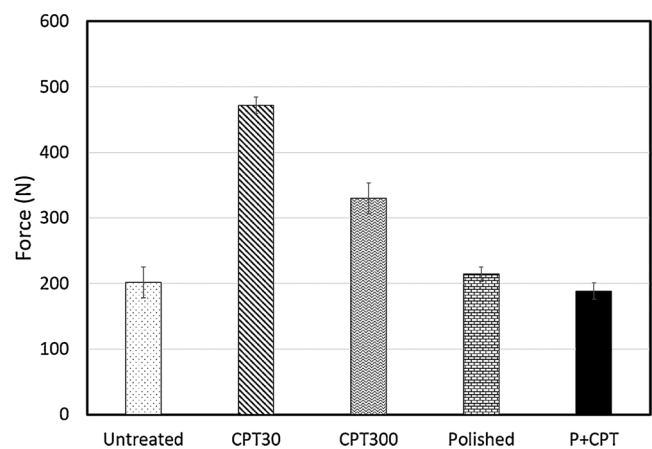


Fig. 10. Comparison of the peak force of all conditions.

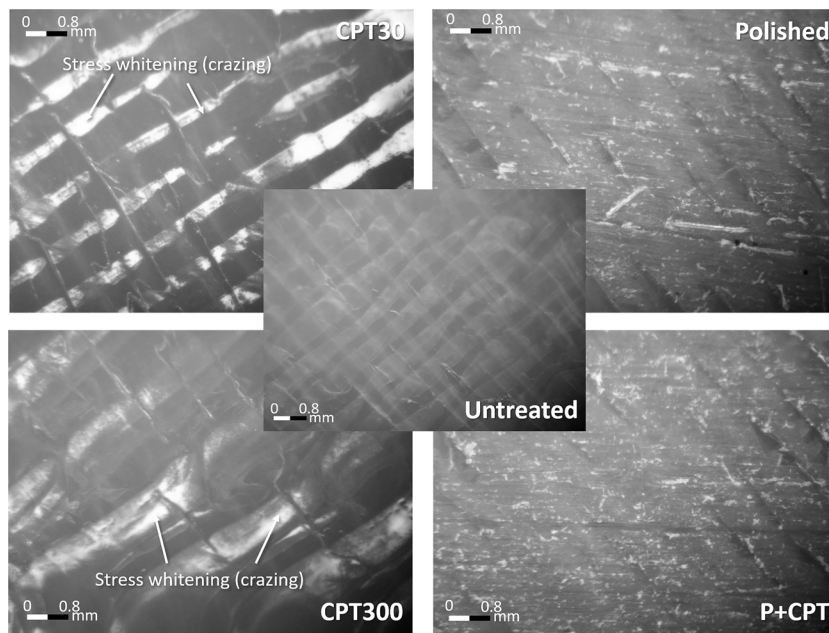


Fig. 11. The microscope observation on the fractured surfaces of different treatments, including untreated, CPT30, CPT300, Polished, and P + CPT.

whitening effect, indicating an easy separation of the top layer. The optical images agree with the force results obtained from the shear bond test in Fig. 10. Note the small and scattered whitening spots in the polished and P + CPT samples were created by abrasives during the polishing process instead of layer separation during the shear bond test.

4. Discussion

As CPT can enhance interlayer bonding in FFF parts, determining an optimized treatment time is desired in order to achieve the best possible performance. According to the results, the specimens treated with shorter CPT are shown to have stronger bonding than the ones which underwent longer treatment. This may be due to polymer degradation caused by overtreatment. When a polymer surface is exposed to plasma, an oxidation layer can grow into the surface at a certain rate over time. As mentioned in Section 1, the oxidized surface is one of the key elements for enhanced surface energy; however, overgrowing the oxidized layer with an excessive thickness (up to 6 μm depending on the treatment time and parameters [5]) may negatively affect the treatment performance. The oxidation layer has a relatively low strength (due to lower molecular weight); thus, a thicker oxidation layer may become a weak intermediate layer that triggers fractures. Therefore, tuning the treatment time duration to reach a certain level of oxidation on target surfaces is an essential task for optimizing bonding strength based on the work-material and plasma parameters.

Another counterintuitive observation is that the wettability was not shown to dominate the bonding strength based on the results of the polished specimens. Unlike common adhesion cases such as paint coating and adhesive bonding that solely rely on chemical bonds, where the wettability (a spontaneous spread-out motion) plays a key role, the viscous or semi-solid polymer used in FFF can hardly deform without

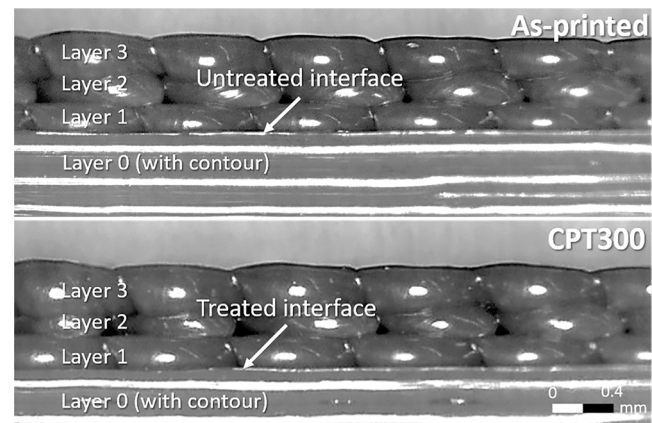


Fig. 12. Mesostructures of the untreated and CPT300 specimens under a microscope. The base layer (layer 0) has a contour line which blocks the deposited material cross-section, while layers 1–3 have the contour line disabled.

external forces. On the other hand, these external forces can overwrite the wettability effects. When the melt is being laid down onto a surface, the surface is melted due to heat transfer and the surface geometry is “mowed.” All while, the printing nozzle squeezes and compresses the melt while printing. These can all change the interfacial contact area significantly more than the wettability can alone.

To further look into the wettability effects, the structures of untreated and CPT300 specimens were observed under a microscope. As shown in Fig. 12, the results show no or little to no difference between

the untreated and treated specimens. In other words, the different initial wetting conditions do not change how the melt spreads on a surface in FFF. Therefore, the wettability may not be a major factor in CPT to enhance the bonding strength of FFF. This observation also explains why the polished surface does not exhibit any improvement despite having a high wettability.

Instead, mechanical polishing seems to worsen the bonding strength. This result may be explained by the removal of printing patterns (Fig. 5) which are made of multiple single extrusion arrays. Such a pattern can potentially provide interlocking between layers through a 45°/45° printing orientation and produce a larger contact area than a smooth surface. This hypothesis can be indirectly verified by the comparison between the polished and P + CPT cases. Although CPT can enhance polymer diffusion, the polishing process that removes the patterns may even out the effect of CPT, thus the overall bonding shows no increase.

Before concluding, there are several limitations applied to this work that should be mentioned. Firstly, the CPT effect is time sensitive and can degrade over time. Although the time between treatment and test was kept short, within 30 min., the actual degradation of treated surfaces was not quantitatively measured. Generally, the plasma effect can last around 24 h or longer [5], so the time interval is considered insignificant. Secondly, only one material (PLA) was tested with a fixed plasma condition; thus the quantitative effects of plasma on the bonding strength, such as treatment time, cannot be generalized. Finally, the comparison between the CPT and polished cases also involve the difference in surface roughness in addition to wettability (which are coupled together). The discussion on wettability effect is based on the assumption that surface interlocking is not dominant.

5. Conclusions

This study determined the improvement of interlayer bonding strength of 3D printed PLA parts treated by cold plasma. A low-energy plasma system and shear bonding apparatus were specifically built to meet the needs of the experimental design. Based on the results, it was found that CPT can significantly increase the bonding strength by over 100%, which is likely to bring the z-direction strength closer to that of the x- and y-directions of the printed part. Longer treatment is not necessarily better, however, and there should exist an optimal treatment setting for different thermoplastics used. Another important finding is that the dominant mechanism for CPT to enhance the interlayer bonding is polymer scission instead of wettability. A counterpart specimen with a better wettability caused by mechanical polishing resulted in no improvement to weaker bonding.

This study has successfully demonstrated the positive effect of CPT in FFF while also unveiling possibly sophisticated mechanisms behind the CPT based 3D printing process. Before the optimization of CPT is possible, fundamental studies on both chemical, mechanical, and combined mechanisms are necessary.

References

- [1] S.S. Crump, USPTO (Ed.), Apparatus and Method for Creating Three-Dimensional Objects, Stratasys Inc., USA, 1989.
- [2] A. Sung-Hoon, M. Michael, O. Dan, R. Shad, W.P. K., Anisotropic material properties of fused deposition modeling ABS, *Rapid Prototyp. J.* 8 (4) (2002) 248–257.
- [3] C. Bellehumeur, L. Li, Q. Sun, P. Gu, Modeling of bond formation between polymer filaments in the fused deposition modeling process, *J. Manuf. Process.* 6 (2) (2004) 170–178.
- [4] A.C. Abbott, G.P. Tandon, R.L. Bradford, H. Koerner, J.W. Baur, Process-structure-property effects on ABS bond strength in fused filament fabrication, *Addit. Manuf.* 19 (2018) 29–38.
- [5] S. Wu, Polymer Interface and Adhesion, Marcel Dekker, New York, 1982.
- [6] T.J. Coogan, D.O. Kazmer, Bond and part strength in fused deposition modeling, *Rapid Prototyp. J.* 23 (2) (2017) 414–422.
- [7] V.E.S. Kuznetsov, A.N. A.G. Tavtov, O.D. Urzhumtsev, A.H. Vakulik, Increasing of Strength of FDM (FFF) 3D Printed Parts by Influencing on Temperature-Related Parameters of the Process, Preprints, (2018).
- [8] H. Abouraya, P. Dobbyn, D. Dowling, Enhancing the mechanical performance of additive manufactured polymer components using atmospheric plasma pre-treatments, *Plasma Process. Polym.* 15 (3) (2018) 1700141.
- [9] N.A. Nguyen, C.C. Bowland, A.K. Naskar, A general method to improve 3D-printability and inter-layer adhesion in lignin-based composites, *Appl. Mater. Today* 12 (2018) 138–152.
- [10] A.K. Ravi, A. Deshpande, K.H. Hsu, An in-process laser localized pre-deposition heating approach to inter-layer bond strengthening in extrusion based polymer additive manufacturing, *J. Manuf. Process.* 24 (2016) 179–185.
- [11] V. Kishore, C. Ajinjeru, A. Nycz, B. Post, J. Lindahl, V. Kunc, C. Duty, Infrared preheating to improve interlayer strength of big area additive manufacturing (BAAM) components, *Addit. Manuf.* 14 (2017) 7–12.
- [12] C.B. Sweeney, B.A. Lackey, M.J. Pospisil, T.C. Achee, V.K. Hicks, A.G. Moran, B.R. Teipel, M.A. Saed, M.J. Green, Welding of 3D-printed carbon nanotube–polymer composites by locally induced microwave heating, *Sci. Adv.* 3 (6) (2017).
- [13] S. Shaffer, K. Yang, J. Vargas, M.A. Di Prima, W. Voit, On reducing anisotropy in 3D printed polymers via ionizing radiation, *Polymer* 55 (23) (2014) 5969–5979.
- [14] A. Garg, A. Bhattacharya, A. Batish, Chemical vapor treatment of ABS parts built by FDM: analysis of surface finish and mechanical strength, *Int. J. Adv. Manuf. Technol.* 89 (5) (2017) 2175–2191.
- [15] W. Jo, O.-C. Kwon, M.-W. Moon, Investigation of influence of heat treatment on mechanical strength of FDM printed 3D objects, *Rapid Prototyp. J.* 24 (3) (2018) 637–644.
- [16] G. Li, J. Zhao, W. Wu, J. Jiang, B. Wang, H. Jiang, J. Fuh, Effect of ultrasonic vibration on mechanical properties of 3D printing non-crystalline and semi-crystalline polymers, *Materials* 11 (5) (2018) 826.
- [17] A. Armillotta, M. Bellotti, M. Cavallaro, Warpage of FDM parts: experimental tests and analytic model, *Robot. Comput. Manuf.* 50 (2018) 140–152.
- [18] E. Bormashenko, G. Whyman, V. Miltanen, E. Shulzinger, G. Chaniel, Physical mechanisms of interaction of cold plasma with polymer surfaces, *J. Colloid Interface Sci.* 448 (2015) 175–179.
- [19] A. Jordá-Vilaplana, V. Fombuena, D. García-García, M.D. Samper, L. Sánchez-Nácher, Surface modification of polylactic acid (PLA) by air atmospheric plasma treatment, *Eur. Polym. J.* 58 (2014) 23–33.
- [20] H. Narahara, Y. Shirahama, H. Koresawa, Improvement and Evaluation of the Interlaminar Bonding Strength of FDM Parts by Atmospheric-Pressure Plasma, *Procedia Cirp* 42 (2016) 754–759.
- [21] L. Bárdos, H. Baránková, Cold atmospheric plasma: sources, processes, and applications, *Thin Solid Films* 518 (23) (2010) 6705–6713.
- [22] J. Chang, P.A. Lawless, T. Yamamoto, Corona discharge processes, *Ieee Trans. Plasma Sci.* 19 (6) (1991) 1152–1166.
- [23] S.A. Dion, A.S. David, F. Alexander, F. Bakhshian, Atmospheric pressure dc corona discharges: operating regimes and potential applications, *Plasma Sources Sci. Technol.* 18 (3) (2009) 035016.
- [24] I.G. Valentin, J.P. Gerhard, The development of dielectric barrier discharges in gas gaps and on surfaces, *J. Phys. D Appl. Phys.* 33 (20) (2000) 2618.
- [25] U. Kogelschatz, Dielectric-barrier discharges: their history, discharge physics, and industrial applications, *Plasma Chem. Plasma Process.* 23 (1) (2003) 1–46.
- [26] B. Ronny, Dielectric barrier discharges: progress on plasma sources and on the understanding of regimes and single filaments, *Plasma Sources Sci. Technol.* 26 (5) (2017) 053001.
- [27] J. Winter, R. Brandenburg, K.D. Weltmann, Atmospheric pressure plasma jets: an overview of devices and new directions, *Plasma Sources Sci. Technol.* 24 (6) (2015) 064001.
- [28] S.K. Pankaj, C. Bueno-Ferrer, N.N. Misra, V. Milosavljević, C.P. O'Donnell, P. Bourke, K.M. Keener, P.J. Cullen, Applications of cold plasma technology in food packaging, *Trends Food Sci. Technol.* 35 (1) (2014) 5–17.
- [29] T. Dufour, J. Minnebo, S.A. Rich, E.C. Neyts, A. Bogaerts, F. Reniers, Understanding polyethylene surface functionalization by an atmospheric He/O₂ plasma through combined experiments and simulations, *J. Phys. D Appl. Phys.* 47 (22) (2014) 224007.
- [30] K. Terpiłowski, D. Rymuszka, Surface free energy changes of polyethylene after plasma treatment, in: A. Mendez-Vilas, A. Solano-Martin (Eds.), *Polymer Science: Research Advances, Practical Applications and Educational Aspects*, Formatec Research Center, Spain, 2016, pp. 498–505.
- [31] K. Cantekin, S. Avcı, Evaluation of shear bond strength of two resin-based composites and glass ionomer cement to pure tricalcium silicate-based cement (Biodentine®), *J. Appl. Oral Sci.* 22 (2014) 302–306.

- [32] C. Laux, Radiation and Nonequilibrium Collisional-radiative Models, (2000).
- [33] S. David, F. Bakhtier, F.G. Alexander, A.F. Alexander, Spectroscopic studies and rotational and vibrational temperature measurements of atmospheric pressure normal glow plasma discharges in air, *Plasma Sources Sci. Technol.* 15 (4) (2006) 818.
- [34] A. International, ASTM D7334-08(2013) Standard Practice Ffor Surface Wettability of Coatings, Substrates and Pigments by Advancing Contact Angle Measurement, West Conshohocken, PA (2013).
- [35] C.B. Bucknall, R.R. Smith, Stress-whitening in high-impact polystyrenes, *Polymer* 6 (8) (1965) 437–446.